01 Dec 2016

Effect of Amino-Functionalization on Insulin Delivery and Cell Viability for Two Types of Silica Mesoporous Structures

Abdollah Zakeri Siavashani

Masoumeh Haghbin Nazarpak

Fateme Fayyazbakhsh
Missouri University of Science and Technology, f.fba@mst.edu

Tayebeh Toliyat

et. al. For a complete list of authors, see https://scholarsmine.mst.edu/mec_aereng_facwork/5058

Recommended Citation

A. Zakeri Siavashani et al., "Effect of Amino-Functionalization on Insulin Delivery and Cell Viability for Two Types of Silica Mesoporous Structures," *Journal of Materials Science*, vol. 51, no. 24, pp. 10897 - 10909, Springer, Dec 2016.
The definitive version is available at https://doi.org/10.1007/s10853-016-0301-1

J Mater Sci (2016) 51:10897–10909

Effect of amino-functionalization on insulin delivery and cell viability for two types of silica mesoporous structures

Abdollah Zakeri Siavashani[1], Masoumeh Haghbin Nazarpak[2,*], Fateme Fayyazbakhsh[1], Tayebeh Toliyat[3], Steven James Peter McInnes[4], and Mehran Solati-Hashjin[1]

[1] *Faculty of Biomedical Engineering, Amirkabir University of Technology (Tehran Polytechnic), Tehran 15914, Iran*
[2] *New Technologies Research Center (NTRC), Amirkabir University of Technology (Tehran Polytechnic), Tehran 15914, Iran*
[3] *Department of Pharmaceutics, Faculty of Pharmacy, Tehran University of Medical Sciences, Tehran, Iran*
[4] *ARC Centre of Excellence in Convergent Bio-Nano Science and Technology, Mawson Institute, University of South Australia, GPO Box 2471, Adelaide, South Australia 5001, Australia*

Received: 11 July 2016
Accepted: 12 August 2016
Published online: 19 August 2016

ABSTRACT

Inorganic mesoporous structures are a class of novel biomaterials that have shown practical applications in delivery of a variety of therapeutic agents. In the present study, two mesoporous structures were prepared, and the effect of surface modification on their insulin delivery and in vitro cytotoxicity was evaluated. Morphological and structural characterizations of silica particles were accomplished by different analytical techniques, including scanning electron microscopy, X-ray diffraction, Fourier transform infrared spectroscopy (FTIR), and Brunauer–Emmett–Teller (BET) surface area analyses. The drug loading capacity and in vitro drug release behavior of silica structures were investigated under simulated gastrointestinal conditions and phosphate-buffered saline solution using FTIR and UV–Vis spectroscopy. In vitro cytotoxicity evaluation was carried out via MTT assay. Results showed that the morphology of MCM-41 was round, while SBA-15 was wheat like, both possessed almost homogeneous size distribution. Also, modification with amine did not influence the morphology and structure of the particles. Both MCM-41 and SBA-15 particles were found to have narrow pore-size distributions of 2.8 and 6.8 nm, respectively. SBA-15 particles demonstrated a high insulin loading capacity of about 15.1 %, while MCM-41 and modified MCM-41 (mMCM-41) were observed to load virtually no insulin at all. The surface modification by amino groups resulted in higher insulin loading and the slower rate of release for modified SBA-15 (mSBA-15) compared to the non-modified SBA-15 (SBA-15). According to the cytotoxicity evaluation results, all of the samples showed cytotoxicity Grade 0–1, in a concentration-dependent manner. Moreover, insulin-loaded mSBA-15 particles exhibited higher cell viability compared to the others. It was concluded that amine modification of SBA-15 could result in higher loading and extended release of insulin and more cell viability.

Address correspondence to E-mail: haghbin@aut.ac.ir

DOI 10.1007/s10853-016-0301-1

Introduction

At the beginning of the 1990s, the M41S family of ordered mesoporous silica was introduced, and the synthesis of advanced mesoporous materials has undergone explosive growth since then [1]. These novel compositions have many specific applications in areas such as catalysis [2], sorption [3], separation [4], sensing [5], optics [6], diagnostic approaches [7], and drug delivery [8]. Generally, mesoporous materials are derived from supramolecular assemblies of surfactants, which template the inorganic precursor during synthesis. By eliminating the surfactant, different silica phases are obtained. These materials can be easily synthesized by sol–gel methods in acidic or basic conditions containing the silica precursor and the surfactant micelles as the template. The most common and well-known ordered mesoporous frameworks are the 2D hexagonal planar MCM-41 and SBA-15 structures (symmetry group p6mm) with around 2 and 10 nm pores, respectively, and the 3D-cubic MCM-48 (symmetry group la3d) with the pore size of approximately 3 nm [9]. Stable mesoporous structures with well-defined surface properties such as MCM-41 and SBA-15 materials consist of a honeycomb-like porous structure of empty channels that can store relatively large amounts of bioactive molecules. They are ideal for encapsulation of pharmaceutical drugs, proteins, and other biogenic molecules [10]. The use of silica materials for clinical applications has considerably expanded in recent years, in particular for orthopedics [11] and drug delivery systems [10]. Silica-based materials are also used in glass ceramics [12], silica nanospheres [13], and bioglasses [14]. Many researchers have also focused on other types of these materials, such as star gels, template glasses, and ordered mesoporous materials. Initial investigations confirmed that silica materials have the potential for clinical applications [15]. Mesoporous silica particles contain some attractive features, such as high surface area, large pore volume, tunable pore size, uniform porosity, and stability in aqueous media [16, 17].

Recent researches in the synthesis of mesoporous silica materials have led to the development of a series of new delivery systems with various molecules, such as pharmaceutical drugs [18] and fluorescent imaging agents [19, 20]. Their easy chemical functionalization by different organic groups, biocompatibility, and uniformly sized pores and volume has made them useful for many biomedical purposes, such as drug [8] and gene delivery systems [21].

The functionalization by 3-aminopropyltriethoxysilane (APTES) can be accomplished at different temperatures and reaction times and in different solvents, such as toluene and ethanol [22]. In recent years, mesoporous materials for loading and delivery of various pharmaceutical molecules, such as gentamicin [23], ibuprofen [24], amoxicillin [25], and alendronate [26] have been developed. Both small and large molecules can be entrapped within the mesopores [27]. Surface functionalization and geometrical design of the pores are two strategies that allow for the precise control of the chemical surface properties and subsequently determine both drug release and transport properties of the carrier [28].

Peptide delivery has been a significant challenge for the pharmaceutical industry due to factors such as immunogenicity and sensitivity to enzymatic degradation, temperature, and pH variations, leading to short plasma half-lives [29]. Compared with organic carriers, such as liposomes, hydrogels, and polymeric nanoparticles, mesoporous silica possesses better stability [30, 31] and the possibility of avoiding a burst release [32]. Recently, there has been an increased interest toward insulin delivery via inorganic materials such as silica nanoparticles. Andreani et al. developed silica nanoparticles coated with mucoadhesive polymers for oral administration of insulin [33], and they showed that surface engineering of silica nanoparticles may be a promising approach to design carriers for oral administration of proteins [34]. However, silica nanoparticles as drug carriers cannot avoid burst release, and their loading capacity is limited to the surface of particles. Although recently some reports have described the adsorption and release behavior of different small molecular drugs [23, 26] from mesoporous silica, there are only few reports studying peptides adsorption and delivery behavior in mesoporous silica [35–37]. Lin et al. used mesoporous silica for direct delivery of enzymes into cells and showed that mesoporous structures can be promising carriers for the delivery of enzymes [36]. Furthermore, Tukappa et al. introduced a polyglutamic acid-gated mesoporous silica nanoparticle as enzyme carrier for treating cancer cells [37]. Also, Gan et al. provided a pH-responsive mesoporous silica carrier for peptide delivery and showed an excellent capability for protein delivery via SBA-15 mesoporous structures [38]. In our previous work, we investigated the possibility of insulin loading in SBA-15 structure and studied its release behavior for 6 h in simulated gastrointestinal

tract and reported that SBA-15 can be a suitable carrier for peptide drugs such as insulin [39]. Our present approach offers more comprehensive information about this structure as an insulin delivery carrier and an insight into the effect of pore size and surface chemistry modification on insulin loading and release and their effect on cell viability. Although the use of different kinds of mesoporous silica for insulin delivery has been studied previously, it is the first time that a comparison between MCM-41 and SBA-15 and their functionalized form as insulin delivery systems is studied, and their effect on cell viability is evaluated. The aim of amino-functionalization was to improve drug loading capacity and decrease release rate as a result of drug and amino groups interactions and studying its effect on cell viability. The mesoporous silica surfaces were amino-functionalized with APTES by a post-grafting method. Both chemistries were investigated for the storage, and release of insulin in different simulated buffers, such as phosphate-buffered saline (PBS), simulated gastric fluid (SGF) and simulated intestinal fluid (SIF), was investigated.

Materials

Tetraethyl orthosilicate (TEOS, Merck 99/9 %), hexadecyltrimethylammonium bromide (CTAB, Aldrich, 95 %), sodium hydroxide (Aldrich, 98 %), Pluronic P123 (PEG-PPG-PEG, Aldrich Mw 5800), (3-aminopropyl)triethoxysilane (APTES, Aldrich, 99 %), hydrochloric acid (Merck, 37 %), anhydrous toluene (Aldrich, 99.8 %), human insulin of recombinant DNA origin (Exir), Dulbecco's modified Eagle's medium (DMEM, Gibco BRL Life Technologies), fetal bovine serum (FBS, Gibco BRL Life Technologies), and MTT [3-(4,5 dimethylthiazol-2-yl)-2,5-diphenyltetrazolium bromide, Sigma] were all used as received without further purification.

Methods

Mesoporous silica preparation

Preparation of MCM-41

MCM-41 particles were prepared through sol–gel process according to the literature with minor modifications [9, 40]. Briefly, 1.04 g of NaOH was dissolved in 1800 mL of water at 80 °C. Then, 3.71 g of CTAB was added to the solution and stirred vigorously. When the CTAB had completely dissolved, 17.33 g of TEOS was added dropwise. Subsequently, the solution was stirred for 2 h at 80 °C. The resulting precipitate was filtered and washed with water and ethanol. In order to completely remove the CTAB, the particles were calcined at 550 °C for 48 h. Each procedure was repeated many times under the same controlled conditions.

Preparation of SBA-15

SBA-15 particles were prepared through a hydrothermal process by pluronic P123-templated condensation reaction of TEOS according to the literature with minor modifications [18, 22]. Briefly, 4 g of pluronic P123 was dissolved into 150 mL of 2 M HCl solution. Up to 8.5 g of TEOS was then added dropwise to the solution and was stirred continuously at 500 rpm and the reaction temperature was maintained at 35 °C for 20 h. Subsequently, the mixture was aged at 100 °C for 24 h under static conditions in a Teflon-lined autoclave. The precipitated product was then filtered and washed with deionized water and dried at room temperature. Finally, the particles were calcined at 600 °C for 6 h to remove the surfactant. Each procedure was repeated many times under the same controlled conditions.

Functionalization of particles by post-synthesis grafting

To study the influence of amino groups on peptide loading and delivery, mesoporous particles were functionalized by APTES. Functionalization of MCM-41 and SBA-15 with amino groups was accomplished by immersion of particles into 2 mmol APTES in 30 mL of anhydrous toluene at 110 °C for 2 h. The particles were then washed and dried. The obtained samples were designated as mMCM-41 and mSBA-15 [22, 30].

Characterization of mesoporous silica particles

X-ray diffraction

Powder X-ray patterns were carried out using a PANalytical and Equinox 3000 instrument, with Cu K radiation. Typically, the diffractograms have been

collected in the 2θ values in the ranges of 1.5°–10° and 5°–75° at room temperature. In order to support the results, the experiment was repeated three times for random samples.

Scanning electron microscopy

Scanning electron microscopy (SEM) images were obtained on a XL30 field emission SEM (acceleration voltage of 10 kV; Philips). The samples were attached to aluminum stubs and coated with a thin layer of gold before analysis.

Nitrogen adsorption analysis

BET surface area, pore volume, and pore diameter were determined by N_2 adsorption using the BJH method in a Belsorp-mini II.

Fourier transform infrared spectroscopy

Fourier transform infrared spectroscopy (FTIR) was carried out with a BOHEM FT-IR spectrophotometer, scanning from 400 to 4000 cm^{-1} at a resolution of 4 cm^{-1} for 42 consecutive scans at room temperature in KBr pellets.

Insulin loading and release study

Insulin loading was performed by dissolving 4000 units of insulin in 68 mL of 0.1 M acetic acid solution. Once dissolved, 680 mg of mesoporous silica powder was added and stirred for 24 h. Subsequently, the particles were centrifuged at 4000 rpm and the supernatant was collected and its concentration was analyzed by UV–Vis to calculate the amount of drug loading into the particles. The particles were subsequently washed with deionized water for three times. Release studies were performed with 160 mg of drug-loaded mesoporous silica after immersion in 40 mL of simulated gastric fluid (SGF) at pH 1.2 under stirring for 2 h. Then the particles were collected and re-immersed in simulated intestinal fluid (SIF) at pH 6.8 while stirring for another 4 h. The release evaluation in PBS at pH 7.4 was performed using 320 mg of the sample for 10 days. All of the delivery tests were repeated three times. The insulin loading percentage was quantified using UV–Vis spectroscopy and characterized by FTIR spectroscopy [41].

Cytotoxicity evaluation

The cytotoxicity of the samples was evaluated via MTT assay. Caco-2 cells as a human colon epithelial cancer cell line were cultured in 96-well plate at 5×10^3 cells/100 μL medium in each well with Dulbecco's modified Eagle's medium (DMEM), 10 % fetal bovine serum (FBS), 100 U mL^{-1} penicillin, and 100 mg mL^{-1} streptomycin at 37 °C in a humidified atmosphere of 5 % CO_2. Then the cell culture plate was incubated for 24 h to allow cell attachment.

After 24 h exposure to different concentrations of samples, MTT was added to wells and incubated for 4 h. After that, 50 μL of DMSO was added to each well, and the spectrophotometric absorbance of the samples was measured at 570 nm by microplate reader (BioTek ELX808). An average of three measurements was taken for each group.

Results and discussion

The crystalline structure of materials can be determined by X-Ray Diffraction (XRD) of CuKα radiation. We used low-angle XRD to characterize the structure of our mesoporous materials and verify the arrangement of the pores. Although the walls of mesoporous materials generally do not have a crystalline structure, these materials show some peaks in low-angle XRD spectra due to the difference between scattering power of the silica framework and the pore voids [1, 9]. Figure 1 shows the XRD pattern of MCM-41, mMCM-41, SBA-15, and mSBA-15 in both low and high angles. The results of MCM-41 and mMCM-41 at low angles showed the four peaks corresponding to diffraction of (100), (110), (200), and (210) planes (Fig. 1a). SBA-15 and mSBA-15 exhibited three peaks corresponding to the (100), (110), and (200) reticular planes (Fig. 1c) confirming a highly ordered hexagonal mesostructure for each particle, which revealed that the mesoporous silica particles were MCM-41- and SBA-15-type materials, and this hexagonal structure remains unchanged after functionalization. At high angles, XRD patterns of MCM-41 and SBA-15 exhibited amorphous structure of the silica, which is in agreement with previous reports (Fig. 1b–d) [17, 22]. Porous structures can also be characterized by their adsorption–desorption properties. Nitrogen sorption isotherm analysis provides information about the properties of porous materials

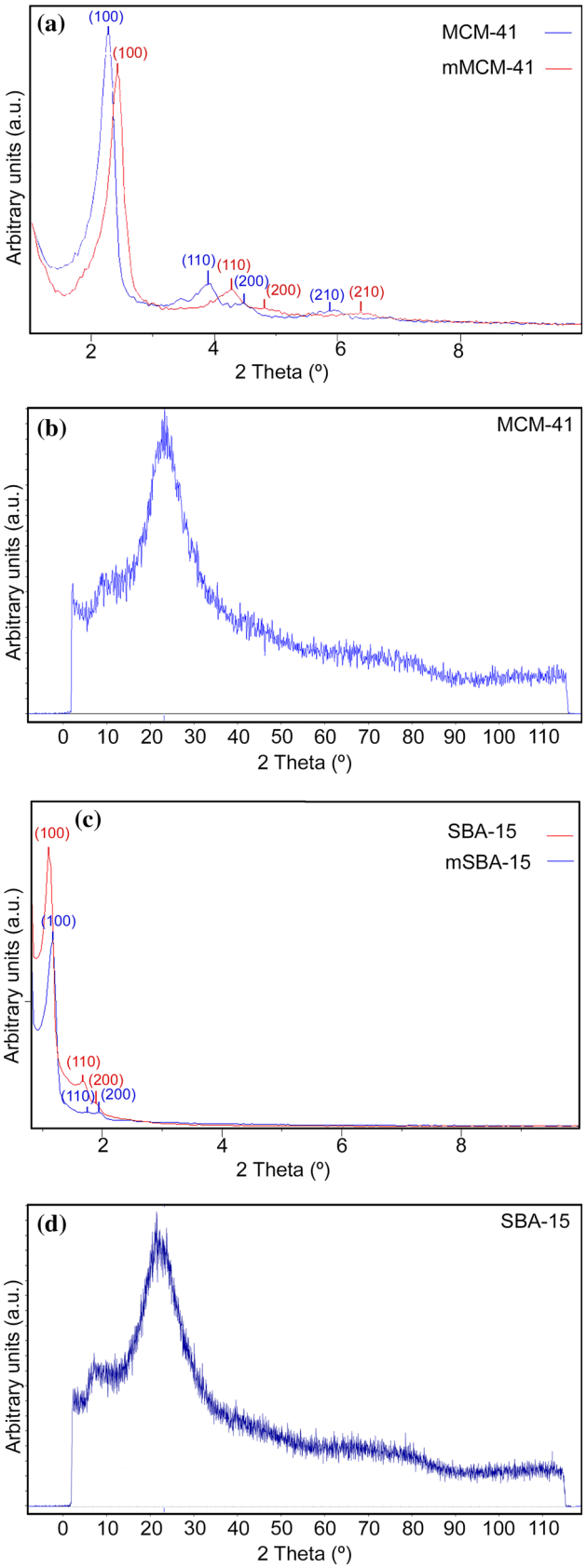

◀**Figure 1** XRD patterns of mesoporous silica particles. **a** Low-angle XRD patterns of MCM-41 and mMCM-41. **b** High-angle XRD pattern of MCM-41. **c** Low-angle XRD patterns of SBA-15 and mSBA-15. **d** High-angle XRD pattern of SBA-15.

via the formation of a monolayer of nitrogen gas on the surface of the porous material. Typically, a pressure range P/P0 between 0.2 and 0.3 is observed for MCM-41 materials and between 0.4 and 0.7 for SBA-15-type materials. The inflection of the isotherm in these ranges demonstrates the capillary condensation inside the pores and a hysteresis loop can be created by the evaporation of nitrogen at a pressure lower than the capillary condensation. Mesoporous structures generally display type IV or V isotherms and solids with well-defined cylindrical-like pore channels and uniform pore sizes provide a type H1 hysteresis, compared to a type H2 hysteresis for

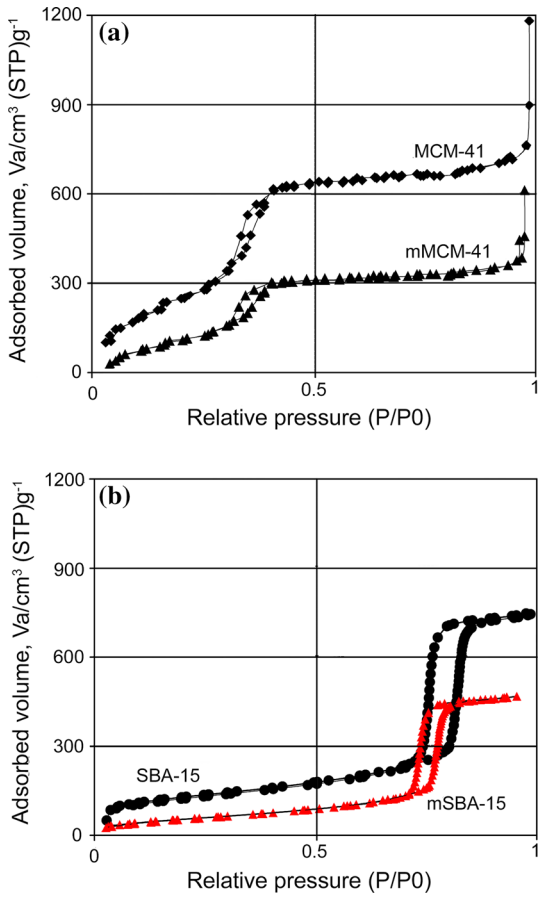

Figure 2 Nitrogen gas adsorption–desorption isotherm of mesoporous silica. **a** MCM-41 and mMCM-41. **b** SBA-15 and mSBA-15. *Va* volume of gas adsorbed at standard temperature and pressure (STP).

disordered and non-uniform pores [42]. The nitrogen sorption isotherms (Fig. 2) show the typical type IV and H1 hysteresis loop for all samples according to the IUPAC classification, which is a typical characteristic of MCM-41 and SBA-15 with well-defined hexagonal cylindrical channels and open uniform pores. The BET surface area, pore volume, and pore size are listed in Table 1. These results are in good agreement with the results of other studies [43, 44]. The pore diameter of MCM-41 and mMCM-41 (2.8 and 2.46 nm) is very close to the size of the insulin molecule and this will influence the ability to load drug into the pores. The pore diameters of SBA-15 and mSBA-15 are larger than the insulin molecule and should make them more amenable for insulin loading. The observed pore size change post surface modification with APTES demonstrates the successful functionalization of the amino group onto the pore walls as a decrease in pore volume, pore diameter, and specific surface area was observed for both mMCM-41 and mSBA-15 compared to MCM-41 and SBA-15. These facts confirm the grafting of the amine group to the pore wall, which causes less available space for adsorbed nitrogen.

Table 1 Results from BET analysis of N_2 gas absorption data for mesoporous silica particles

Sample	SBET (m^2 g^{-1})	Vpore (cm^3 g^{-1})	Pore size (nm)
MCM-41	645	1.38	2.8
SBA-15	449	1.12	6.11
mMCM-41	342	0.97	2.46
mSBA-15	248	0.75	5.73

SEM characterization revealed topographical, compositional, and structural differences within the two materials [43–45]. Figure 3a–d shows SEM images of MCM-41, mMCM-41, SBA-15, and mSBA-15, respectively. These images indicate that MCM-41 and SBA-15 particles have sequentially uniform particle size between the ranges of 200–400 and 300–500 nm and aggregated into the round and wheat-like structure. The SEM images reveal that the samples have the same morphology as commonly observed in this kind of mesoporous materials, and they have long-range parallel channels with 2D-hexagonal mesoporous structure. Importantly, these images also show no change in the morphology of silica after modification with APTES.

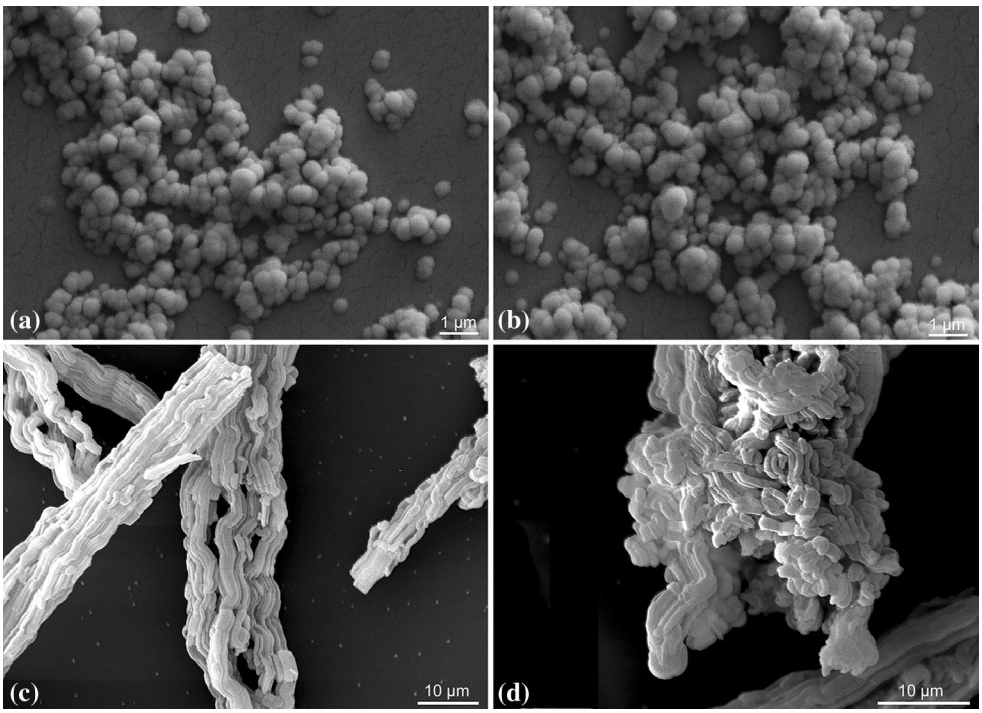

Figure 3 SEM image of mesoporous silica particles. **a** MCM-41. **b** mMCM-41. **c** SBA-15. **d** mSBA-15.

Drug loading capacity and insulin release were quantified in SGF, SIF, and PBS by UV–Vis spectroscopy. To achieve quantification, an insulin standard curve was constructed via serial dilutions of 10–200 μg mL^{-1} and quantification at 270 nm in deionized water, 0.1 M acetic acid solution, SGF, SIF, and PBS. Insulin was loaded into mesoporous silica by immersing porous particles in the insulin solution. The amount of insulin loaded into samples was calculated from the difference in concentration of insulin in the supernatant after particle centrifugation and the initial concentration in the solution used for loading. UV–Vis spectroscopy results showed that MCM-41 absorbed no insulin and mMCM-41 only absorbed 0.8 % of the insulin in the solution, which is due to the small pore sizes (2.8 and 2.46 nm). In contrast, the larger pores (6.06 and 5.73 nm) of the SBA-15 materials were able to absorb 15.1 and 17.6 % of insulin into SBA-15 and mSBA-15, respectively (Fig. 4). According to other research results, it is hypothesized that insulin not only can be adsorbed on the surface of mesoporous structure, but it also can enter into the pores of SBA-15 structure [46, 47].

Despite the decrease in pore size, the higher adsorption capacity of mMCM-41 and mSBA-15 compared to MCM-41 and SBA-15 can be attributed to the insulin adsorption caused by interactions between insulin and functional groups and changes in hydrophilicity which is in agreement with other investigations [48]. Although insulin is considered a large peptide with a molecular diameter of approximately 2.7 nm, the obtained loading results is rather significant and close to the previous published report by Sun et al. [49] and is considerably high compared to other reports of small therapeutic agents. For instance, Rehman et al. reported 18 % loading for ibuprofen which only has a diameter around 0.6 × 1.0 nm [50]. However, because of the variety of mesoporous structures, different kinds of functional groups on surfaces and lack of reports about insulin loading in SBA-15 structure, comparing these results with other reports of insulin loading in SBA-15 structure is rather difficult. For instance, although Choi et al. showed a high insulin loading capacity (76 %) in S-MCF mesoporous silica with pore diameter larger than 20 nm, in comparison with mSBA-15, S-MCF did not release insulin in a controlled way [51]. Moreover, Elsayed et al. developed an injectable insulin-loaded hollow silica, which is also called mesoporous silica nanoparticle, for controlled release of insulin. However, hollow mesoporous particles need to break down to release the drug. Therefore, drug carriers may be excreted by body without releasing their content, and therapeutic agents cannot exert their pharmacological effects [35]. As a result, while considering the extended release of

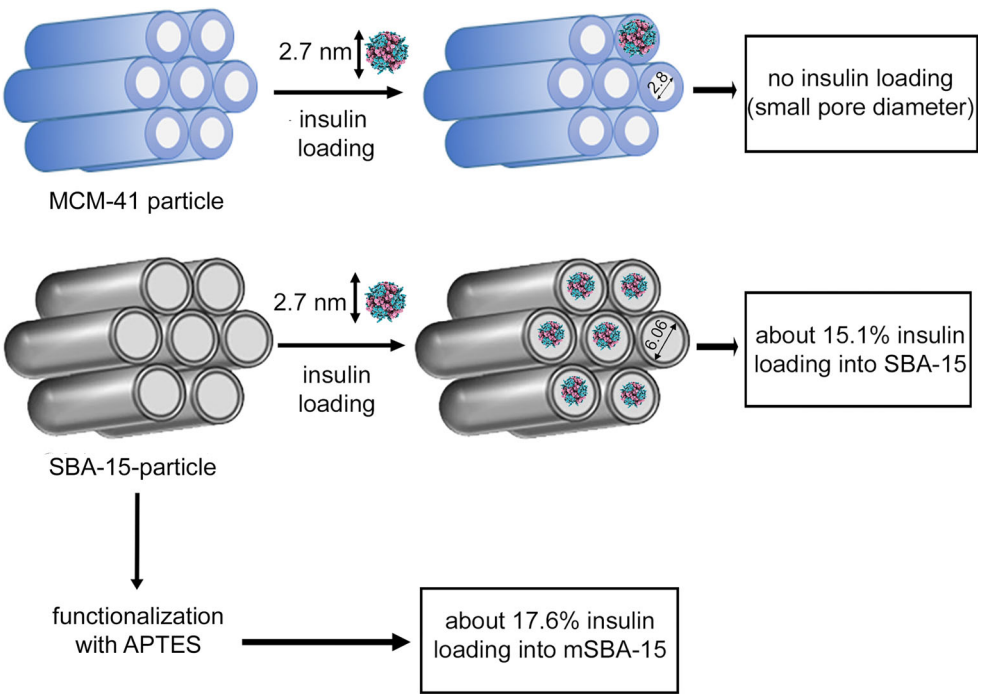

Figure 4 Schematic illustration of drug loading of silica and amine-modified samples.

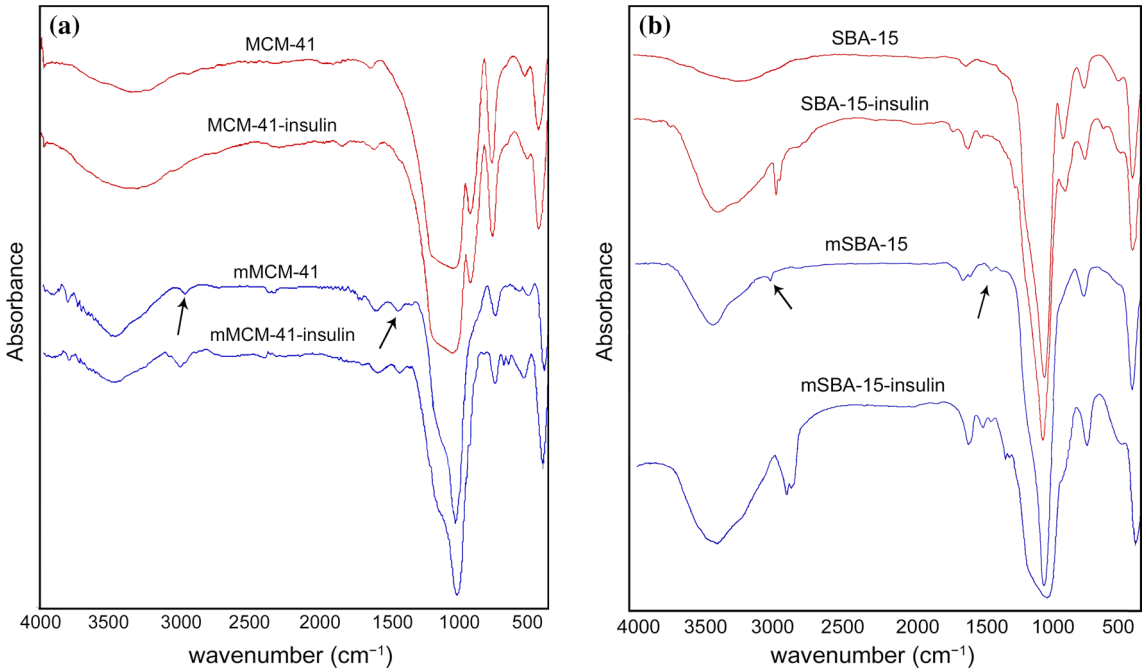

Figure 5 FTIR spectra of **a** MCM-41, mMCM-41, MCM-41-insulin, and mMCM-41-insulin. **b** SBA-15, mSBA-15, SBA-15-insulin, and mSBA-15-insulin.

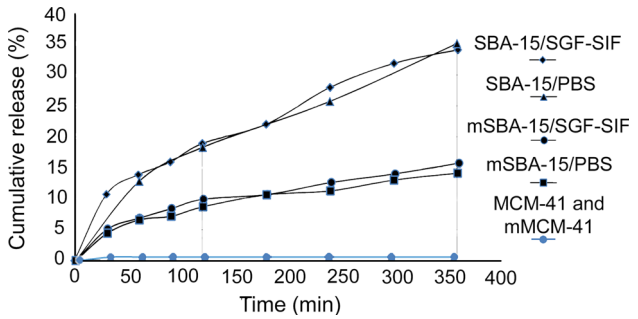

Figure 6 Cumulative insulin release from SBA-15, mSBA-15, MCM-41, and mMCM-41 after 2 h in simulated gastric fluid and after 4 h in simulated intestinal fluid and 6 h in PBS buffer.

insulin, mSBA-15 has a better capacity for controlling insulin release and increasing its blood half-life.

These results confirm that the lower surface area of SBA-15 showed a higher drug loading compared to the MCM-41 having higher surface area which could not load insulin due to pore-size constraints. Insulin loading into the mesoporous structure was also confirmed with FTIR analyses. Figure 5a shows the FTIR spectra of MCM-41 and mMCM-41 before and after drug loading. The characteristic bands located at around 1087 cm^{-1} of MCM-41 are attributed to the asymmetric stretching vibrations of Si–O–Si [27], and the bands around 474 and 791 cm^{-1} of MCM-41 can be assigned to the symmetric stretching and deformation of Si–O–Si [27]. The MCM-41 peaks at 962 cm^{-1} are associated with the bending of Si–OH [27]. The subsequent functionalization of MCM-41 by APTES resulted in the appearance of the bands at 2963 and 1464 cm^{-1}, which can be attributed to the C–H and N–H stretching vibrations of the amino-propyl groups. The FTIR spectrum of MCM-41 insulin-loaded samples shows no new peaks which corroborate the UV–Vis results of no insulin loading. The spectra of mMCM-41 after drug loading shows small peaks around 3395, 1644, and 2890 cm^{-1} can be attributed to the C=O and N–H bands at amides' types I and II in insulin [52].

Figure 5b shows a similar trend of increasing IR spectroscopy peaks for insulin loaded into SBA-15-based materials at an enhanced intensity due to the significantly higher loading.

Figure 6 displays the in vitro release of insulin from SBA-15 and mSBA-15 in SGF, SIF, and PBS. The results show that the release was time dependent. The morphology of SBA-15 with 2D hexagonally structured pores influences the diffusion process in and out of the pores and extends the release of insulin [17]. Approximately, 18.4 % of insulin release was found in the simulated gastric fluid over the first 120 min, and an additional 14.3 % was released in the simulated intestinal fluid over the next 240 min.

Compared with SBA-15, mSBA-15 showed slower insulin release (about 8.7 and 15.79 %) in these buffer solutions over the same duration. However, about half of insulin is entrapped within the porous structure of both samples, which is one of the disadvantages of non-degradable mesoporous ceramics. The rather similar amount of released insulin from both SBA-15 and mSBA-15 in 360 min at PBS, and the simulated gastrointestinal fluid demonstrates that the release rate is not pH dependent and amino-modification does not have any special effect on pH sensitivity.

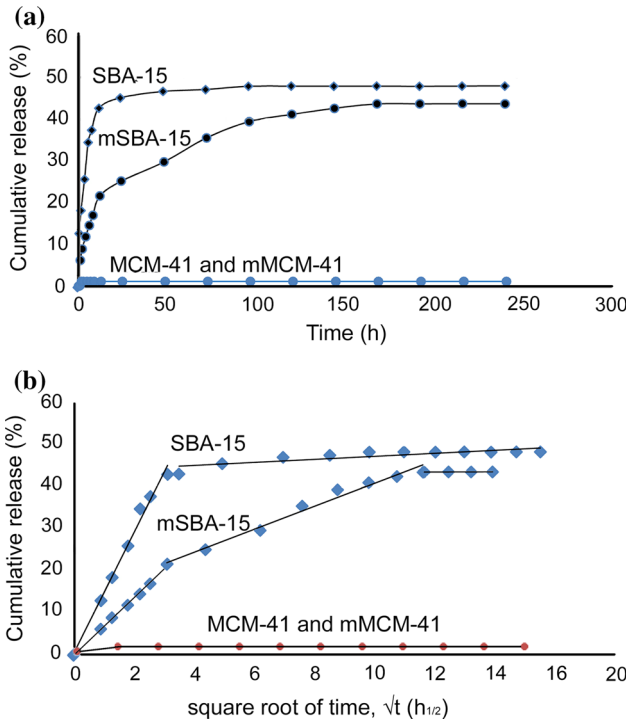

Figure 7 Cumulative insulin release from SBA-15, mSBA-15, mMCM-41, and MCM-41 after 10 days in PBS. **a** Cumulative insulin release as a function of time (h). **b** Cumulative insulin Release as a function of square root of time (h).

Figure 7a shows the extended cumulative insulin release from MCM-41, mMCM-41, SBA-15, and mSBA-15 in PBS for 10 days. In order to analyze the release mechanism, we compared different release models, including zero-order, first-order, and Hixon-Crowell and the Higuchi model (Table 2). These results demonstrated that the best-fit model was Higuchi model. The Higuchi equation focuses on the influence of concentration gradient and is one of the best suitable models of diffusion controlled release from mesoporous materials:

$$Q = k\sqrt{t},$$

where Q is the amount of drug released after time t and k is the Higuchi dissolution constant [21].

This mechanism signifies that the solution fluid penetrates into the silica matrix and diffusion controls the release of insulin. Both of SBA-15 and mSBA-15 matrices display a two-step release (Fig. 7). The initial stage of release in samples is attributed to the dissolution and release of the portion of insulin located near the surface of the pores. Given that insulin is a water-soluble drug, the insulin molecules near the surface and on the outer surface of the particles will be released to the solution medium rather quickly. In SBA-15 sample, silanol groups in silica walls can interact with hydroxyl and amino groups of insulin molecule by hydrogen bonding, which can explain the slow insulin release rate in the later stage. Also, mSBA-15 shows slower release of insulin than SBA-15, which can be explained by chemical interactions of the primary amines on the silica surface and functional groups of insulin molecules.

The cytotoxicity assessment was carried out using Caco-2 cells via MTT assay. The cell viability was calculated according to the following formula:

$$\text{Cell viability}\,(\%) = \text{OD}_{\text{sample}}/\text{OD}_{\text{control}} \times 100$$

where the control group is associated with the proliferation of cells in DMEM medium.

Table 2 Comparison of R2 values of fitting insulin release to different release models

Material		MCM-41 and mMCM-41	SBA-15	mSBA-15
Zero order (h)	12	–	0.8741	0.9196
	12–240	–	0.6836	0.8377
First order (h)	12	–	0.9195	0.9394
	12–240	–	0.586	0.804
Higuchi (h)	12	–	0.9906	0.9977
	12–240	–	0.8217	0.9813
Hixson-Crowell (h)	12	–	0.9227	0.9236
	12–240	–	0.454	0.7823

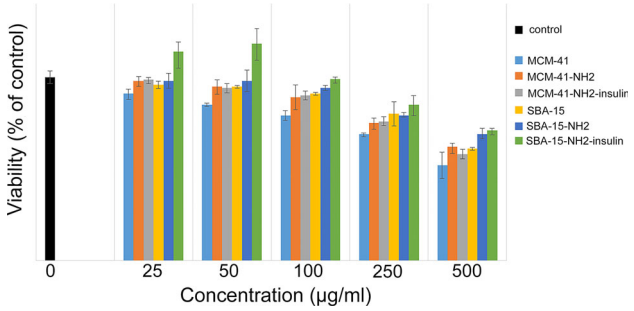

Figure 8 MTT results for samples using Caco-2 cells. *Error bars* represent the standard deviation from three repeated experiments.

According to Fig. 8, all of the samples have the cytotoxicity Grade 0–1 (ISO 10993-5). It can be seen that cytotoxicity depends on concentration. In all samples, the number of viable cells will decrease with the increasing concentrations. Moreover, the higher cell viability of SBA-15 compared to MCM-41 particles can be attributed to larger surface area of MCM-41 structure. In fact, Li et al. [53] have shown that by increasing the surface area of silica particles, they produce more oxidative stress, which leads to higher cytotoxicity. According to our present work, particles with size between 200 and 500 nm are expected to have higher cell viability than nanoparticles which can be explained by lower cell membrane penetration of larger particles and their lower surface area [53].

On the other hand, the cells exposed to insulin-loaded samples show the highest absorbance. These good results can be attributed to the effective role of insulin in cell culture which works as a growth factor and can improve cell survival. The better cell viability of amino-modified samples is in accordance with the report of Lankoff et al. [54], who reported that modification of silica can reduce ROS induction and makes them safer for medical application.

Furthermore, it seems that amino-functionalization may have a positive effect on cell viability. This observation has been reported by several authors in different types of cell lines and materials [55, 56]. In fact, it has been indicated that surface chemistry plays an important role in particle and cell interactions and protein adsorption [57, 58]. Li et al. reported that increase in amino density improves the proliferation of neural stem cells [55]. Moreover, Chen et al. suggested that positively charged hydroxyapatite nanoparticles can improve cell viability and cell proliferation in comparison with neutral surfaces [58]. On the other hand, Chung et al. proved the effect of positively charged surfaces on biological function of mesenchymal stem cells [59]. This effect can be attributed to improvement of electrostatic interactions between amine groups and negative charges on cell surface which can influence particle binding to cells and subsequent cell signaling.

Conclusion

In this study, the possibility of peptide loading into two types of mesoporous silica structures and consequent drug release was analyzed. The effect of surface modification by amine groups was investigated and the effect of amino-modification on insulin delivery and cell cytotoxicity was evaluated. Results showed that MCM-41 and SBA-15 structures were successfully prepared using sol–gel and hydrothermal methods, and functionalization was performed with APTES by post-synthesis grafting. SBA-15 particles showed more insulin loading capacity compared to MCM-41, which did not absorb insulin molecules. This can be attributed to the small ratio of insulin diameter to pore diameter. Hence, the careful choice of pore size is crucial for obtaining adequate drug loading.

The modification of SBA-15 with APTES also leads to an increase in loading content of the particles and a slower release rate than that of SBA-15. However, no significant difference was observed for insulin loading and release in MCM-41 and mMCM-41. The results of in vitro cell viability experiment indicated that samples show the cytotoxicity Grade 0–1 in a concentration-dependent manner. Most importantly, SBA-15 samples show higher cell viability than MCM-41, and it was indicated that mSBA-15-insulin would promote cell proliferation.

Although, this work confirms that amine-modified SBA-15 mesoporous nanostructures are promising materials for peptide delivery, several aspects of in vitro tests remain to be elucidated and optimized.

Acknowledgements

This study was supported by the Iran National Science Foundation (INSF) Grant No. 91002648.

References

[1] Webster JG (2006) Encyclopedia of medical devices and instrumentation, 2nd edn. Wiley, New York

[2] Yokoi T, Kubota Y, Tatsumi T (2012) Amino-functionalized mesoporous silica as base catalyst and adsorbent. Appl Catal A 42:14–37. doi:10.1016/j.apcata.2012.02.004

[3] Chung J, Chun J, Lee J, Lee SH, Lee YJ, Hong SW (2012) Sorption of Pb(II) and Cu(II) onto multi-amine grafted mesoporous silica embedded with nano-magnetite: effects of steric factors. J Hazard Mater 239–240:183–191. doi:10.1016/j.jhazmat.2012.08.063

[4] Cabot A, Arbiol J, Cornet A, Morante JR, Chen F, Liu M (2003) Mesoporous catalytic filters for semiconductor gas sensors. Thin Solid Films 436:64–69. doi:10.1016/S0040-6090(03)00510-8

[5] Tomer VK, Adhyapak PV, Duhan S, Mulla IS (2014) Humidity sensing properties of Ag-loaded mesoporous silica SBA-15 nanocomposites prepared via hydrothermal process. Microporous Mesoporous Mater 197:140–147. doi:10.1016/j.micromeso.2014.06.007

[6] Börgardts M, Verlinden K, Neidhardt M, Wöhrle T, Herbst A, Laschat S, Janiak C, MüllerSynthesis TJJ (2016) Synthesis and optical properties of covalently bound Nile Red in mesoporous silica hybrids—comparison of dye distribution of materials prepared by facile grafting and by co-condensation routes. RSC Adv 6:6209–6222. doi:10.1039/C5RA22736D

[7] Kempen PJ, Greasley S, Parker KA, Campbell JL, Chang HY, Jones JR, Sinclair R, Gambhir SS, Jokerst JV (2015) Theranostic mesoporous silica nanoparticles biodegrade after pro-survival drug delivery and ultrasound/magnetic resonance imaging of stem cells. Theranostics 5:631–642. doi:10.7150/thno.11389

[8] Maggini L, Cabrera I, Ruiz-Carretero A, Prasetyanto E, Robinet E, De Cola L (2016) Breakable mesoporous silica nanoparticles for targeted drug delivery. Nanoscale 7:7240–7247. doi:10.1039/C5NR09112H

[9] He Q, Gao Y, Zhang L, Zhang Z, GaoF Ji X, Li Y, Shi J (2011) A pH-responsive mesoporous silica nanoparticles-based multi-drug delivery system for overcoming multi-drug resistance. Biomaterials 32:7711–7720. doi:10.1016/j.biomaterials.2011.06.066

[10] Wang S (2009) Ordered mesoporous materials for drug delivery. Microporous Mesoporous Mater 117:1–9. doi:10.1016/j.micromeso.2008.07.002

[11] Wang S, Wang X, Draenert FG, Albert O, Schroder HC, Mailander V, Mitov G, Muller WE (2014) Bioactive and biodegradable silica biomaterial for bone regeneration. Bone 67:292–304. doi:10.1016/j.bone.2014.07.025

[12] Persson C, Unosson E, Ajaxon I, Engstrand J, Engqvist H, Xia W (2012) Nano grain sized zirconia–silica glass ceramics for dental applications. J Eur Ceram Soc 32:4105–4110. doi:10.1016/j.jeurceramsoc.2012.06.028

[13] Li J, Qin X, Yang Z, Qi H, Xu Q, Diao G (2013) A novel mesoporous silica nanosphere matrix for the immobilization of proteins and their applications as electrochemical biosensor. Talanta 104:116–121. doi:10.1016/j.talanta.2012.11.038

[14] Xia L, Zeng D, Sun X, Xu Y, Xu L, Ye D, Zhang X, Jiang X, Zhang Z (2013) Engineering of bone using rhBMP-2-loaded mesoporous silica bioglass and bone marrow stromal cells for oromaxillofacial bone regeneration. Microporous Mesoporous Mater 173:155–165. doi:10.1016/j.micromeso.2013.02.020

[15] Mamaeva V, Sahlgren C, Lindén M (2013) Mesoporous silica nanoparticles in medicine—Recent advances. Adv Drug Deliv Rev 65:689–702. doi:10.1016/j.addr.2012.07.018

[16] Gimenez C, de la Torre C, Gorbe M, Aznar E, Sancenón F, Murguía JR, Martínez-Máñez R, Marcos MD, Amorós P (2015) Gated mesoporous silica nanoparticles for the controlled delivery of drugs in cancer cells. Langmuir 31:3753–3762. doi:10.1021/acs.langmuir.5b00139

[17] Bhattacharyya S, Wang H, Ducheyne P (2012) Polymer-coated mesoporous silica nanoparticles for the controlled release of macromolecules. Acta Biomater 8:3429–3435. doi:10.1016/j.actbio.2012.06.003

[18] Xue J, Shi M (2004) PLGA/mesoporous silica hybrid structure for controlled drug release. J Controlled Release 98:209–217. doi:10.1016/j.jconrel.2004.04.023

[19] Chen X, Yao X, Wang C, Chen L, Chen X (2015) Mesoporous silica nanoparticles capped with fluorescence-conjugated cyclodextrin for pH-activated controlled drug delivery and imaging. Microporous Mesoporous Mater 217:46–53. doi:10.1016/j.micromeso.2015.06.012

[20] Qu Y, Feng L, Tong C, Liu B, Lu C (2013) Poly (p-phenylenevinylene) functionalized fluorescent mesoporous silica nanoparticles for drug release and cell imaging. Microporous Mesoporous Mater 182:155–164. doi:10.1016/j.micromeso.2013.08.045

[21] Slowing II, Vivero-Escoto JL, Wu CW, Lin VS (2008) Mesoporous silica nanoparticles as controlled release drug delivery and gene transfection carriers. Adv Drug Deliv Rev 60:1278–1288. doi:10.1016/j.addr.2008.03.012

[22] Xu Y, Wang C, Zhou G, Wu Y, Chen J (2012) Improving the controlled release of water-insoluble emodin from amino-functionalized mesoporous silica. Appl Surf Sci 258:6366–6372. doi:10.1016/j.apsusc.2012.03.041

[23] Doardio AL, Sousa SE, Doadrio JC, Pariente JP, Izquierdo-Barba I, Vallet-Regi M (2014) Mesoporous SBA-15 HPLC evaluation for controlled gentamicin drug delivery. J Controlled Release 97:125–132. doi:10.1016/j.jconrel.2004.03.005

[24] Ghedini E, Signoretto M, Pinna F, Guarascio D, Cerrato G (2008) Ibuprofen delivery behaviour on MCM–41: influence of organic groups amount. Stud Surf Sci Catal 174:429–432. doi:10.1016/S0167-2991(08)80234-0

[25] Airoldi C, Oliveira VV (2014) Hydrophobic contribution to amoxicillin release associated with organofunctionalized mesoporous SBA-16 carriers. Mater Res Bull 59:214–222. doi:10.1016/j.materresbull.2014.06.031

[26] Huang W, Liu W, She Z, Wu H, Shi X (2011) Alendronate decorated nano hydroxyapatite in mesoporous silica: cytotoxicity and osteogenic properties. Appl Surf Sci 257:9757–9761. doi:10.1016/j.apsusc.2011.06.002

[27] Al-Kady AS, Gaber M, Hussein MM, Ebeid EZM (2011) Nanostructure-loaded mesoporous silica for controlled release of coumarin derivatives: a novel testing of the hyperthermia effect. Eur J Pharm Biopharm 77:66–74. doi:10.1016/j.ejpb.2010.10.007

[28] Wang H, Gao X, Wang Y, Wang J, Niu X, Deng X (2012) Effect of amine functionalization of SBA-15 on controlled baicalin drug release. Ceram Int 38:6931–6935. doi:10.1016/j.ceramint.2012.05.062

[29] Mahato RI, Narang AS, Thoma L, Miller DD (2003) Emerging trends in oral delivery of peptide and protein drugs. Crit Rev Ther Drug Carr Syst 20:164–167. doi:10.1615/CritRevTherDrugCarrierSyst.v20.i23.30

[30] Wang H, Zhao P, Su W, Wang S, Liao Z, Niu R, Chang J (2010) PLGA/polymeric liposome for targeted drug and gene co-delivery. Biomaterials 31:8741–8748. doi:10.1016/j.biomaterials.2010.07.082

[31] Forier K, Raemdonck K, De Smedt SC, Demeester J, Coenye T, Braeckmans K (2014) Lipid and polymer nanoparticles for drug delivery to bacterial biofilms. J Controlled Release 190:607–623. doi:10.1016/j.jconrel.2014.03.055

[32] Park K (2014) Controlled drug delivery systems: past forward and future back. J Controlled Release 190:3–8. doi:10.1016/j.jconrel.2014.03.054

[33] Andreani T, Miziara L, Lorenzón EN, de Souza AL, Kiill CP, Fangueiro JF, Garcia ML, Gremião PD, Silva AM, Souto EB (2015) Effect of mucoadhesive polymers on the in vitro performance of insulin-loaded silica nanoparticles: interactions with mucin and biomembrane models. Eur J Pharm Biopharm 93:118–126. doi:10.1016/j.ejpb.2015.03.027

[34] Andreani T, Kiill CP, de Souza AL, Fangueiro JF, Fernandes L, Doktorovová S, Santos DL, Garcia ML, Gremião MP, Souto EB, Silva AM (2014) Surface engineering of silica nanoparticles for oral insulin delivery: characterization and cell toxicity studie. Colloids Surf B 123:916–923. doi:10.1016/j.colsurfb.2014.10.047

[35] Elsayed A, Al-Remawi M, Maghrabi I, Hamaidi M, Jaber N (2014) Development of insulin loaded mesoporous silica injectable particles layered by chitosan as a controlled release delivery system. Int J Pharm 461:448–458. doi:10.1016/j.ijpharm.2013.12.014

[36] Lin YH, Chen YP, Liu TP, Chien FC, Chou CM, Chen CT, Mou CY (2016) Approach To Deliver Two Antioxidant Enzymes with Mesoporous Silica Nanoparticles into Cells. ACS Appl Mater Interfaces 8:17944–17954. doi:10.1021/acsami.6b05834

[37] Tukappa A, Ultimo A, da la Torre C, Pardo T, Sancenon F, Martinez-Manez R (2016) Polyglutamic acid-gated mesoporous silica nanoparticles for enzyme-controlled drug delivery. Langmuir. doi:10.1021/acs.langmuir.6b01715

[38] Gan Q, Zhu J, Yuan Y, Liu C (2016) pH-Responsive Fe3O4 nanopartilces-capped mesoporous silica supports for protein delivery. J Nanosci Nanotechnol 16:5470–5479. doi:10.1166/jnn.2016.11744

[39] Siavashani AZ, Nazarpak MH, Fayyazbakhsh F, Toliyat T, Solati-Hashjin M (2014) Preparation of mesoporous silica nanoparticles for insulin drug delivery. Adv Mater Res 829:251–257. doi:10.4028/www.scientific.net/AMR.829.251

[40] Chen F, Zhu Y (2012) Chitosan enclosed mesoporous silica nanoparticles as drug nano-carriers: sensitive response to the narrow pH range. Microporous Mesoporous Mater 150:83–89. doi:10.1016/j.micromeso.2011.07.023

[41] Zhang Y, Wei W, Lv P, Wang L, Ma G (2011) Preparation and evaluation of alginate–chitosan microspheres for oral delivery of insulin. Eur J Pharm Biopharm 77:9–11. doi:10.1016/j.ejpb.2010.09.016

[42] Vallet-Regí M, Balas F (2008) Silica materials for medical applications. Open Biomed Eng J 2:1–9. doi:10.2174/1874120700802010001

[43] Pootawang P (2011) Solution plasma synthesis and characteristic for mesoporous silica and metal nanoparticles system. Dissertation, Nagoya University, Nagoya

[44] Szegedi A, Popova M, Goshev I, Mihály J (2011) Effect of amine functionalization of spherical MCM-41 and SBA-15 on controlled drug release. J Solid State Chem 184:1201–1207. doi:10.1016/j.jssc.2011.03.005

[45] Talebian N, Zare E (2014) Structure and antibacterial property of nano-SiO2 supported oxide ceramic. Ceram Int 40:281–287. doi:10.1016/j.ceramint.2013.05.135

[46] Jangra S, Girotra P, Chhokar V, Tomer VK, Sharma AK, Duhan S (2016) In vitro drug release kinetics studies of mesoporous SBA–15-azathioprine composite. J Porous Mater 23:679–688. doi:10.1007/s10934-016-0123-1

[47] Hillerstrom A, Andersson M, Samuelsson J, van Stam J (2014) Solvent strategies for loading and release in mesoporous silica. Colloids Interface Sci Commun 3:5–8. doi:10.1016/j.colcom.2015.01.001

[48] Popova MD, Szegedi A, Kolev LN, Mihaly J, Tzankov BS, Momekov GT, Lambov NG, Yoncheva KP (2012) Carboxylic modified spherical mesoporous silicas as drug delivery carriers. Int J Pharm 436:778–785. doi:10.1016/j.ijpharm.2012.07.061

[49] Sun L, Zhang X, Zheng C, Wu Z, Li CA (2013) pH gated, glucose-sensitive nanoparticle based on worm-like mesoporous silica for controlled insulin release. J Phys Chem B 117:3852–3860. doi:10.1021/jp400442x

[50] Rehman F, Volpe PL, Airoldi C (2014) The applicability of ordered mesoporous SBA-15 and its hydrophobic glutaraldehyde-bridge derivative to improve ibuprofen-loading in releasing system. Colloids Surf B 119:82–89. doi:10.1016/j.colsurfb.2014.03.043

[51] Choi SR, Jang DJ, Kim S, An S, OhE Lee J, Kim J (2014) Polymer-coated spherical mesoporous silica for pH-controlled delivery of insulin. J Mater Chem B 2:616–619. doi:10.1039/C3TB21494J

[52] Mukhopadhyay P, Sarkar K, Chakraborty M, Bhattacharya S, Mishra R, Kundu PP (2013) Oral insulin delivery by self-assembled chitosan nanoparticles: in vitro and in vivo studies in diabetic animal model. Mater Sci Eng C 33:376–382. doi:10.1016/j.msec.2012.09.001

[53] Li Y, Jin M, Du Z, Liu X, Guo C, Li Y, Huang P, Sun Z (2011) Size-dependent cytotoxicity of amourphous silica nanoparticles in human hepatoma HepG2 cells. Toxicol In Vitro 25:1343–1352. doi:10.1016/j.tiv.2011.05.003

[54] Lankoff A, Arabski M, Wegierek-Ciuk A, Kruszewski M, Lisowska H, Banasik-Nowak A, Rozga-Wijas K, Wojewodzka M, Slomkowski S (2013) Effect of surface modification of silica nanoparticles on toxicity and cellular uptake by human peripheral blood lynphocytes in vitro. Nanotoxicology 7:235–250. doi:10.3109/17435390.2011.649796

[55] Li HL, Zhang H, Huang H, Liu ZQ, Li YB, Yu H, An YH (2013) The effect of amino density on the attachment, migration, and differentiation of rat neural stem cells in vitro. Mol Cells 35:436–443. doi:10.1007/s10059-013-0046-5

[56] Hopper AP, Dugan JM, Gill AA, Fox OJ, May PW, Haycock JW, Claeyssens F (2014) Amine functionalized nanodiamond promotes cellular adhesion, proliferation and neurite outgrowth. Biomed Mater. doi:10.1088/1748-6041/9/4/045009

[57] Singh SK, Singh MK, Kulkarni PP, Sonkart VK, Gracio JJA, Dash D (2012) Amine-modified graphene: thrombo-protective safer alternative to graphene oxide for biomedical applications. ACS Nano 6:2731–2740. doi:10.1021/nn300172t

[58] Chen L, Mccrate JM, Lee JC, Li H (2011) The role of surface charge on the uptake and biocompatibility of hydroxyapatite nanoparticles with osteoblast cells. Nanotechnology. doi:10.1088/0957-4484/22/10/105708

[59] Chung TH, Wu SH, Yao M, Lu CW, Lin YS, Hung Y, Mou CY, Chen YC, Huang DM (2007) The effect of surface charge on the uptake and biological function of mesoporous silica nanoparticles in 3T3-L1 cells and human mesenchymal stem cells. Biomaterials 28:2959–2966. doi:10.1016/j.biomaterials.2007.03.00